coatings

MDPI

Article

Shell of *Viviparid* Snail as an Eco-Friendly Corrosion Inhibitor for Carbon Steel in 1 M HCl

Qihui Wang [1,*], Chongkang Zhao [1], Huahao Zheng [1], Qi Zhang [1], Xing Zhou [1], Ruozhou Wang [1], Zhitao Yan [1,*], Yi Sun [1] and Xueming Li [2]

[1] School of Civil Engineering and Architecture, Chongqing University of Science and Technology, Chongqing 401331, China; 2021206071@cqust.edu.cn (C.Z.); 2021206062@cqust.edu.cn (H.Z.); 2021206083@cqust.edu.cn (Q.Z.); 2022206103@cqust.edu.cn (X.Z.); 2022206060@cqust.edu.cn (R.W.); sunyi@cqust.edu.cn (Y.S.)

[2] School of Chemistry and Chemical Engineering, Chongqing University, Chongqing 400044, China; xuemingli@cqu.edu.cn

* Correspondence: qihuiwang@cqust.edu.cn (Q.W.); yzt@cqust.edu.cn (Z.Y.); Tel.: +86-157-2325-0306 (Q.W.); +86-135-5230-3950 (Z.Y.)

Abstract: The shell of *viviparid* snail extract (SVSE) was prepared by a simple and environmentally friendly hydrolysis method and the corrosion inhibition of carbon steel (CS) by SVSE in 1 M HCl was investigated. HPLC and FTIR analysis showed that the main component of SVSE was a mixture of various amino acids. The results of electrochemical and surface analysis showed that SVSE is a hybrid corrosion inhibitor with a corrosion inhibition efficiency of 95.23%. In addition, the adsorption behavior of SVSE on CS surfaces was also investigated in depth by adsorption isotherms, quantum chemistry (QC) and molecular dynamics simulations (MDS).

Keywords: corrosion inhibition; amino acids; waste; adsorption isotherms; EIS; Tafel

check for updates

Citation: Wang, Q.; Zhao, C.; Zheng, H.; Zhang, Q.; Zhou, X.; Wang, R.; Yan, Z.; Sun, Y.; Li, X. Shell of *Viviparid* Snail as an Eco-Friendly Corrosion Inhibitor for Carbon Steel in 1 M HCl. *Coatings* **2023**, *13*, 1136. https://doi.org/10.3390/coatings13071136

Academic Editor: Paweł Nowak

Received: 2 June 2023
Revised: 12 June 2023
Accepted: 21 June 2023
Published: 22 June 2023

1. Introduction

Steel plays a vital role in social production [1]. Because of its active chemical nature, steel experiences inevitable corrosion at all stages of production, transport and storage [2–5]. As a result, corrosion products must be removed from their surface before use [6–8]. Removing corrosion products by pickling is the easy way [9–11]. Corrosion products on the steel surface are removed during the pickling process through dissolution, mechanical stripping, and reduction [12–15]. During the pickling process, the acidic solution not only reacts with the rust layer, but also causes damage to the steel matrix [16–20]. In addition, hydrogen embrittlement caused by the diffusion of H-atoms into the iron during pickling can lead to serious quality defects [21–23]. Corrosion protection researchers have found the addition of corrosion inhibitors to the pickling medium to be among the cost-effective solutions to this problem.

The three types of corrosion inhibitors are inorganic, organic, and polymer based [24–26]. The components of inorganic corrosion inhibitors include chromate, nitrite, silicate, molybdate, and polyphosphate [27,28]. The major components of organic corrosion inhibitors include sulfonated lignin and benzothiazole [29,30]. Polymer compounds such as polyaspartic acid are the primary constituents of polymer-based corrosion inhibitors [31]. The abovementioned corrosion inhibitors suffer from drawbacks such as high cost, environmental harm, and hard deterioration [32]. Recently, corrosion inhibitor development has shifted toward eco-friendly green biomass corrosion inhibitors.

Corrosion prevention researchers have performed a lot of research in the development and application of green corrosion inhibitors. Currently, plant extract corrosion inhibitors are obtained from plant sources such as *Asteraceae* [33], eucalyptus leaves [34], walnut leaves [8], golden bamboo leaves [35], camphor leaves [36], *Andrographis paniculata* [37], rice

bran [38], *Jatropha curcas* [39], green tea tree [40] and cola tree [41]. In addition, amino acid corrosion inhibitors have the merits of being easily available, low cost, and renewable [13]. They can be produced from protein decomposition, which can be totally destroyed in the environment [42]. The radical-paired electrons located in amino acid molecules can react with Fe empty orbitals to establish an adsorption layer [19]. This adsorption layer can significantly reduce the corrosion rate. However, there is a lack of publications on the extraction of amino acid corrosion inhibitors from animal waste proteins.

In this work, SVSE were extracted from the shell of viviparid snail by a facile method. The corrosion inhibition behavior of SVSE on CS in 1 M HCl was investigated in detail by electrochemical impedance spectroscopy (EIS) and potentiodynamic polarization (PDP). In addition, adsorption isotherms, QC calculations and MDS were performed to illustrate the adsorption behavior of SVSE. This work provides a promising avenue for the development of biomass amino acid corrosion inhibitors.

2. Materials and Methods

2.1. Materials

2.1.1. Carbon Steel

The elemental composition of the CS was C (0.160), Si (0.080), Mn (0.210), P (0.015), S (0.012) (wt%), and Fe (residuals). The CS electrode is shaped as a cube with a side length of 1.0 cm. Furthermore, five sides of the electrode were encapsulated with epoxy resin, leaving just 1.0 cm^2 of working area for testing. CS specimens with dimensions of 0.5 cm × 0.5 cm × 0.5 cm were utilized for surface characterization. The test samples were polished with SiC sandpaper (200~7000#).

2.1.2. Test Solutions

The 1 M HCl was configured with 37% HCl and deionized water. The as-prepared SVSE was dissolved into 1 M HCl to prepare 50, 100, 200, and 500 mg/L test solutions. HCl and absolute ethanol were purchased from Kelong Industrial Inc. (Xianyang, China).

2.2. Methods

2.2.1. Preparation of SVSE Extract

In this study, amino acid corrosion inhibitors were prepared using waste *viviparid* snail (*Cipangopaludina chinensis*) as raw materials via a simple hydrolytic process. Firstly, the shell of *viviparid* snail was repeatedly rinsed with deionized water and crushed to a powder. Then, 100 g powder was added to a 70% ethanol solution and stirred at 333 K for 2 h to remove the oil. The precipitate was obtained by centrifugation and then adjusted to 200 mL with a fixed volume of deionized water, and 2.0 g of papain was added. The mixture was stirred at 323 K for 3 h, then heated to 363 K for 15 min to inactivate papain. The supernatant was extracted by centrifugation and freeze dryer for 48 h to obtain the shell of *viviparid* snail extract (SVSE).

2.2.2. Component Analysis

HPLC was used to clarify the chemical composition of SVSE. The instrument was a Shimadzu LC–20AD high-performance liquid chromatograph (Shimadzu, Beijing, China). The mobile phase was prepared by 0.1 M sodium acetate solution, water and acetonitrile, and the column: C 18 (4.6 × 250 mm, 5 μm), column temperature 313 K; flow rate 1 mL/min; characteristic wavelength 254 nm. FTIR was used to further clarify the information on the extracts such as groups and functional groups, and the FTIR test range was 4000~400 cm^{-1}.

2.2.3. Electrochemical Measurements

Electrochemical measurements were performed on a three-electrode system with a CHI660E electrochemical workstation (Shanghai Chenhua Co., Ltd., Shanghai, China). The CS electrode was used as the working electrode, and a Pt sheet was used as the counter electrode. The reference electrode is an SCE electrode. EIS tests were performed at sinusoidal

voltages of 10 mV amplitude (vs. OCP) in the frequency range of 100 kHz–10 mHz. The EIS test results were analyzed using ZsimpWin software (version 3.30, AMETEK, Berwyn, PA, USA). The range of the potentiodynamic polarization test was −250 mV to +250 mV, with a scan rate of 1 mV/s. The polarization test data were obtained by Tafel extrapolation.

2.2.4. Surface Characterization

For surface observation, each CS sample was carefully sanded with SiC sandpaper (200~7000#) and then degreased with absolute ethanol. The samples were soaked in 1 M HCl containing different concentrations of SVSE for 2 h each and then rinsed and dried, followed by SEM observation.

2.2.5. Quantum Chemical Calculations

All parameter calculations for quantum chemistry are performed with the Gaussian 09W program. The planar structures of the molecules were drawn using ChemDraw 19.0 software, and the molecular structures were optimized using the GaussView5 program. Geometric configuration, full optimization and quantum chemical calculations were performed for each corrosion inhibitor molecule at the B3LYP\6–311+G (d, p) level using DFT theory. The formulae for some important parameters are as follows [43–45]:

$$A = -E_{LUMO} \tag{1}$$

$$I = -E_{HOMO} \tag{2}$$

$$\chi = \frac{I + A}{2} \tag{3}$$

$$\gamma = \frac{I - A}{2} \tag{4}$$

$$\Delta N = \frac{\chi_{Fe} - \chi_{inh}}{2(\gamma_{Fe} + \gamma_{inh})} \tag{5}$$

$$\Delta E = I - A \tag{6}$$

where E_{HOMO} is the highest occupied molecular orbital energy, E_{LUMO} is the lowest unoccupied molecular orbital energy, A denotes the electron affinity, I is the ionization potential, γ is the global hardness, ΔN is the electron transfer fraction, χ denotes the electronegativity, and ΔE is the energy gap value.

2.2.6. Molecular Dynamics Simulation

Molecular dynamics simulations were performed using the Forcite module feature in Materials Studio 2018 software (Accelrys, San Diego, CA, USA). First, a model is constructed containing a layer of iron atoms (Fe (110) 6 × 6 × 6), a solution layer (500 H_2O and 1 corrosion inhibitor molecule) and a vacuum layer. Then the model was geometrically optimized (all iron atomic layers were frozen, COMPASS was used for the force field, Smart was used for the algorithm, and Fine was used for the accuracy), and finally the model was simulated with a time step of 1.0 fs for a total simulation time of 1000 ps using the NVT system synthesis for molecular dynamics. The interaction energy ($E_{interact}$) is calculated as follows [46]:

$$E_{intercat} = E_{tot} - E_{sub} - E_{inh} \tag{7}$$

E_{tot} represents the total energy of the whole system, E_{inh} is the total energy of the corrosion inhibitor, and E_{sub} represents the energy of all H_2O molecules and the CS substrate. In addition, the binding energy ($E_{binding}$) is calculated by the following equation [47]:

$$E_{binding} = -E_{interact} \tag{8}$$

3. Results

3.1. FTIR Analysis

From Figure 1, it can be seen that the infrared spectrum of SVSE exhibits multiple absorption peaks in the range of 4000–400 cm^{-1}. Among them, the broad peak at 3500–3000 cm^{-1} is caused by the stretching vibration of O–H/N–H/C–H functional groups in SVSE. The bands observed at 1647 cm^{-1} and 1400 cm^{-1} are attributed to the stretching vibrations of C=O and N–H, respectively. Additionally, the three absorption peaks at 1080 cm^{-1}, 1031 cm^{-1}, and 579 cm^{-1} are mainly due to the stretching vibrations of C–O and C–N, as well as the bending vibration of N–H. It can be concluded that SVSE contains some unique functional groups. The empty orbitals of these organic functional groups can effectively adsorb onto the surface of CS, ultimately slowing down its corrosion [48].

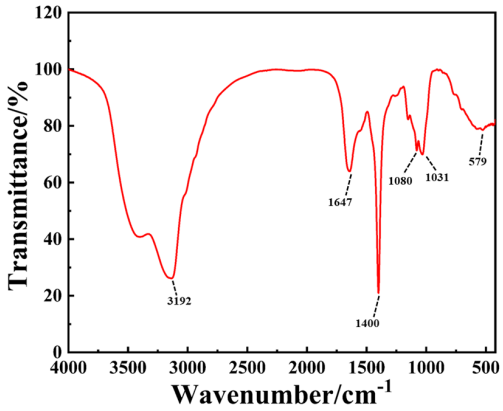

Figure 1. FTIR spectrum of SVSE.

3.2. HPLC Analysis

The content, concentration, and retention time of various amino acids in SVSE after hydrolysis were measured using HPLC, and the information is presented in Table 1, and the chromatogram is displayed in Figure 2. It was detected that SVSE contains 18 types of amino acids, with a total amino acid content accounting for over 24%. High–content amino acids such as Glutamic acid and Aspartic acid accounted for 4.413% and 3.184%, respectively. Numerous existing literature reports have indicated that amino acid molecules can adsorb to metal surfaces through functional groups such as carboxyl, amino, and side chains, thus providing a protective effect on metals. Therefore, the HPLC test results confirm the potential of SVSE as a corrosion inhibitor.

Table 1. Detailed amino acid parameters of SVSE samples.

No.	Ingredient Name	Molecular Formula	CAS No.	Retention Time (min)	Concentration (%)
1	Aspartic acid	$C_4H_7NO_4$	6899–3–2	4.58	3.184
2	Glutamic acid	$C_5H_9NO_4$	6893–26–1	5.213	4.413
3	Hydroxyproline	$C_5H_9NO_3$	6912–67–2	7.908	0.173
4	Serine	$C_3H_7NO_3$	56–45–1	10.215	1.709
5	Glycine	$C_2H_5NO_2$	56–40–6	11.053	1.340
6	Histidine	$C_6H_9N_3O_2$	71–00–1	11.549	0.371
7	Arginine	$C_6H_{14}N_4O_2$	74–79–3	13.333	1.339
8	Threonine	$C_4H_9NO_3$	72–19–5	14.499	1.373
9	Alanine	$C_3H_7NO_2$	6898–94–8	15.253	1.419
10	Proline	$C_5H_9NO_2$	147–85–3	16.089	1.221
11	Tyrosine	$C_9H_{11}NO_3$	55520–40–6	21.721	1.019
12	Valine	$C_5H_{11}NO_2$	7004–03–7	23.118	1.314
13	Methionine	$C_5H_{11}O_2NS$	348–67–4	24.241	0.142
14	Cystine	$C_6H_{12}N_2O_4S_2$	24645–67–8	26.032	0.174
15	Isoleucine	$C_6H_{13}NO_2$	131598–62–4	26.926	1.033
16	leucine	$C_6H_{13}NO_2$	61–90–5	27.371	1.657
17	Phenylalanine	$C_9H_{11}NO_2$	62056–68	29.602	0.928
18	Lysine	$C_6H_{14}N_2O_2$	56–87–1	32.069	1.303

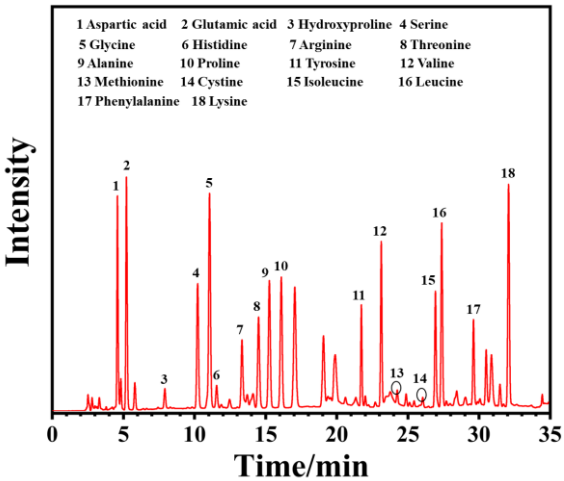

Figure 2. HPLC spectrum of SVSE.

3.3. EIS Analysis

To elucidate the corrosion process of CS in HCl, EIS tests were performed (20 min OCP tests were performed prior to EIS). As shown in Figure 3, the shape of the Nyquist plot did not change with increasing SVSE concentration, indicating that the addition of SVSE did not have an effect on the corrosion mechanism of CS in HCl. Furthermore, these capacitive arcs display incomplete semicircular shapes, which are typically caused by the uneven surface of CS (dispersion effect) [49]. In addition, the radius of the capacitive arc increased with the concentration of SVSE at the four tested temperature conditions. This indicates that increasing the concentration of SVSE facilitates the adsorption of SVSE on the CS surface, while SVSE exhibits good inhibition at higher temperatures. At the same SVSE concentration, the increase in temperature leads to a decrease in the diameter of the capacitive arc. This is due to the fact that the increase in temperature promotes the thermal motion of SVSE molecules, leading to an enhanced effect of SVSE desorption on the CS surface [23].

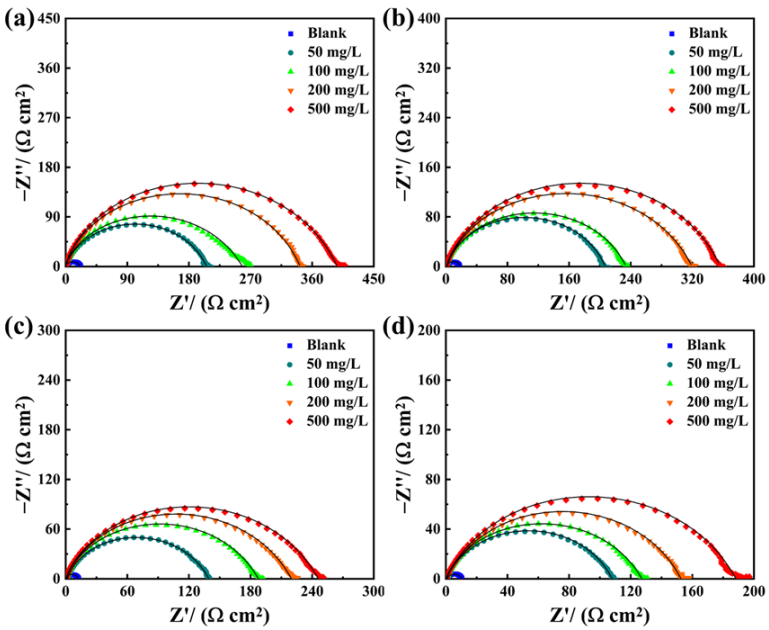

Figure 3. Nyquist plots of the effect of SVSE on the impedance behavior of CS in 1 M HCl: (**a**) 298 K, (**b**) 303 K, (**c**) 308 K, and (**d**) 313 K.

Figure 4 presents the Bode plot of electrochemical impedance. The modulus and phase angle increased significantly with the addition of SVSE, and this phenomenon continued to be amplified with the increase in SVSE concentration. This is because SVSE contains a large number of heteroatoms such as N and O, which can form a protective film on the surface of CS through physical adsorption modes such as electrostatic adsorption and chemisorption modes such as bonding of lone pairs of electrons of its heteroatoms with metal vacant orbitals. The formation of an adsorption film on the CS surface prevents charge transfer from occurring. This further confirms the effective corrosion inhibition of CS by SVSE in a 1 M HCl.

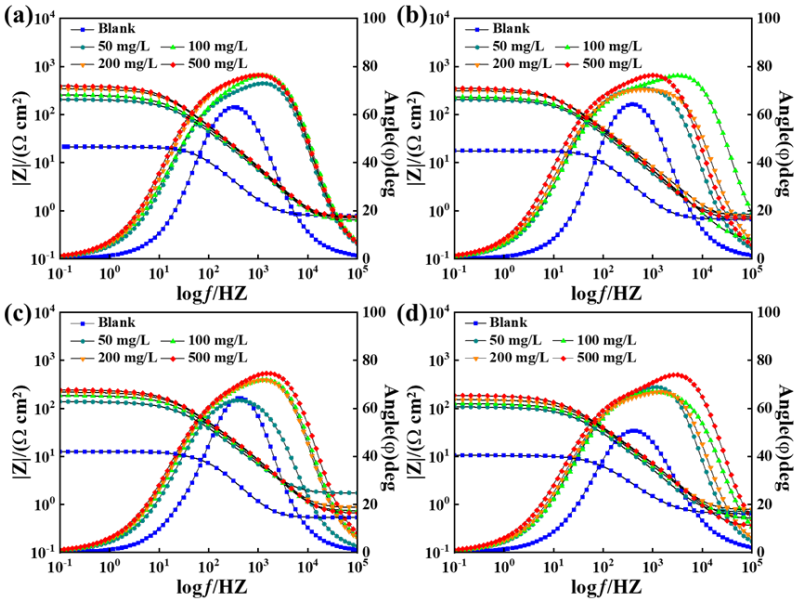

Figure 4. Bode plots of the effect of SVSE on the impedance behavior of CS in 1 M HCl: (**a**) 298 K, (**b**) 303 K, (**c**) 308 K, and (**d**) 313 K.

The microscopic reaction process can be better explained through an equivalent circuit. In the phase angle plot, it can be observed that the angular frequency curve of the blank solution has only one maximum value (one time constant), while the angular frequency curve of the solution containing SVSE has two maximum values (two time constants) [44]. Therefore, two equivalent circuits in Figure 5a,b are used to fit the impedance data without SVSE and with SVSE solution, respectively. Table 2 shows the meaning of each part of the equivalent circuit.

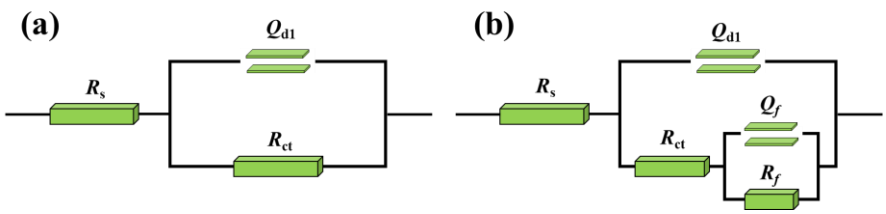

Figure 5. Schematic diagram of the fitted circuit. (**a**) Blank solution, (**b**) Solutions containing SVSE.

Table 2. Specific information of the fitted circuit.

R_S	R_{ct}	R_f	Q_{d1}	Q_f
Solution resistance	Charge transfer resistance	Film resistance	Double-layer capacitance	Membrane capacitance

The corrosion inhibition efficiency (η_R%) of SVSE can be determined by the polarization resistance (R_p), which is calculated as shown in Equation (9). The value of the polarization resistance R_p^0 of the blank solution is equal to R_{ct}, and the value of the polarization resistance R_p of the solution containing SVSE is equal to the sum of the value of its R_{ct} and the value of its R_f. The corrosion inhibition efficiency is calculated by the following equation [50]:

$$\eta_R(\%) = \frac{R_p - R_p^0}{R_p} \times 100 \quad (9)$$

Table 3 shows the relevant electrochemical test results. The largest increase in R_{ct} with increasing SVSE concentration indicates that the charge transfers process controls the corrosion of CS in HCl. The increase in the value of R_p is mainly due to the formation of a film by the corrosion inhibitor molecules on the electrode surface, leading to an increase in resistance. In addition, the value of Q_{dl} decreases with the addition of SVSE due to the adsorption of organic molecules with smaller dielectric constants on the CS surface [51]. The appearance of Q_f and R_f after the addition of SVSE indicates that the electrode surface is covered by a high coverage film [52]. The corrosion inhibition efficiency of SVSE is maintained at a high level of about 95% in the temperature range of 298–313 K. It indicates that the high coverage of the corrosion inhibitor film effectively inhibits the corrosion of CS in HCl.

Table 3. Fitted data of electrochemical impedance spectra.

Temperature	C	R_s	R_f	CPE_{d1}		R_{ct}	CPE_f		η_R
(K)	(mg/L)	(Ω cm^2)	(Ω cm^2)	Y_0 ($\mu\ \Omega^{-1}$ s^n cm^{-2})	n_1	(Ω cm^2)	Y_0 ($\mu\ \Omega^{-1}$ s^n cm^{-2})	n_2	(%)
298 K	Blank	7.87	–	198.3	0.94	20.58	–	–	–
	50	0.71	20.63	20.62	1.00	188.90	150.10	0.69	90.18
	100	0.64	31.52	19.60	1.00	227.30	148.90	0.67	92.05
	200	0.72	36.48	18.52	1.00	306.70	83.90	0.72	94.00
	500	0.75	34.74	17.88	1.00	363.00	83.80	0.71	94.83
303 K	Blank	6.07	–	196.1	0.94	17.16	–	–	–
	50	0.84	14.67	23.99	1.00	190.90	123.00	0.72	91.65
	100	0.25	12.3	18.42	1.00	220.70	123.40	0.72	92.64
	200	0.76	11.34	15.09	1.00	307.00	100.80	0.72	94.61
	500	0.71	36.02	21.97	1.00	320.80	118.20	0.70	95.19
308 K	Blank	0.36	–	165.9	1.00	11.81	–	–	–
	50	1.74	8.33	19.80	1.00	129.80	160.70	0.70	91.45
	100	0.74	18.63	18.72	1.00	168.10	161.00	0.68	93.68
	200	0.87	22.23	17.24	1.00	196.60	128.80	0.70	94.60
	500	0.66	26.74	17.05	1.00	220.60	149.70	0.68	95.23
313 K	Blank	0.64	–	522.9	0.85	9.90	–	–	–
	50	0.71	13.76	27.24	1.00	93.74	221.80	0.71	90.79
	100	0.51	4.06	17.64	1.00	123.00	185.90	0.70	92.21
	200	0.79	12.05	18.63	1.00	140.20	169.80	0.71	93.50
	500	0.36	13.18	18.11	1.00	175.40	172.80	0.70	94.75

3.4. PDP Analysis

The polarization curves were tested using the same solution, temperature and electrode as the EIS test, and the results are shown in Figure 6.

As can be seen from Figure 6, the cathode and anode current densities decreased significantly after the addition of corrosion inhibitor. With increasing concentration of the corrosion inhibitor, the current density continues to decrease regularly. This indicates that the addition of SVSE simultaneously inhibits both cathodic and anodic reactions [53]. With the increase in SVSE concentration, the corrosion potential shows both negative and positive shifts, but the negative shift is greater than the positive shift, indicating a stronger inhibition on the cathodic reaction. Therefore, SVSE can be classified as a mixed-type corrosion inhibitor with a predominant effect on cathodic inhibition [54]. The shape and slope of the polarization curves under different temperature conditions do not change with the addition of SVSE, indicating that SVSE does not alter the corrosion reaction mechanism of the working electrode.

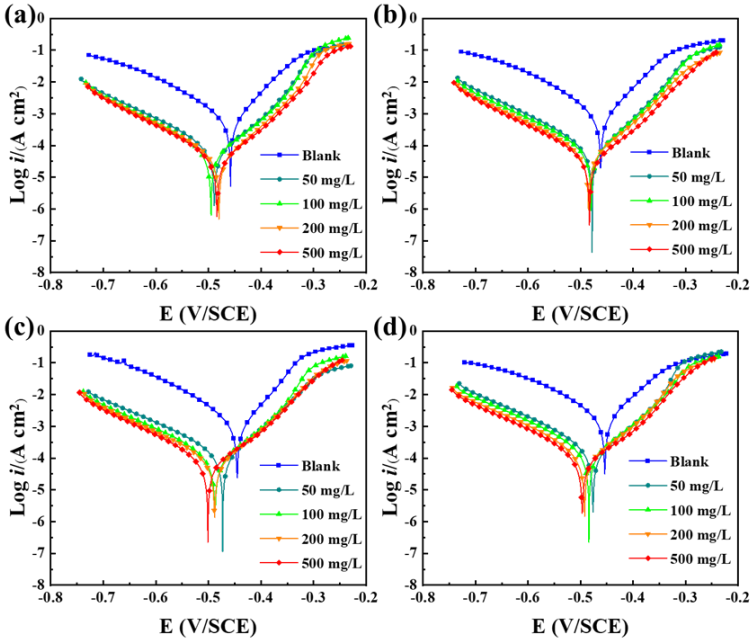

Figure 6. Plots of polarization curves for the effect of different concentrations of SVSE on the potential of CS in 1 M HCl: (**a**) 298 K, (**b**) 303 K, (**c**) 308 K, and (**d**) 313 K.

Table 4 shows the electrochemical parameters for the polarization curve tests. In Table 4, E_{corr} and i_{corr} represent the corresponding corrosion potentials and currents, and β_a and β_c each correspond to the slopes of the anode and cathode of the polarization curves. The maximum displacement of corrosion potential for CS under four temperature conditions were 47 mV, 23 mV, 56 mV and 46 mV (all less than 85 mV), which further indicates that SVSE is a hybrid corrosion inhibitor. The corrosion inhibition efficiency can be calculated by Equation (10) [55]:

$$\eta_p(\%) = \frac{i^0_{corr} - i_{corr}}{i^0_{corr}} \times 100 \tag{10}$$

Table 4. Parameters of interest for polarization curve testing.

Temperature (K)	C (mg/L)	E_{corr} (mV/SCE)	i_{corr} (μA cm^{-2})	$-\beta_c$ (mV dec^{-1})	β_a (mV dec^{-1})	η_p (%)
298 K	Blank	−458	594.4	104.9	62.5	–
	50	−489	62.2	116.3	65.8	89.5
	100	−495	53.7	114.1	71.8	91.0
	200	−480	38.9	114.3	64.9	93.5
	500	−484	35.3	114.9	69.7	94.1
303 K	Blank	−462	774.4	104.5	60.4	–
	50	−478	61.9	114.1	60.0	92.0
	100	−480	58.4	119.1	63.3	92.5
	200	−485	46.7	118.0	67.4	94.0
	500	−483	36.6	119.3	69.7	95.3
308 K	Blank	−445	902.2	102.5	48.7	–
	50	−473	108.9	124.0	68.1	87.9
	100	−488	80.4	122.5	67.8	91.1
	200	−488	70.3	122.5	69.3	92.2
	500	−501	65.8	118.8	79.8	92.7
313 K	Blank	−451	1805.0	115.2	73.5	–
	50	−476	139.2	115.7	65.3	92.3
	100	−484	130.7	118.2	72.7	92.8
	200	−492	98.8	117.4	71.6	94.5
	500	−497	84.6	117.7	78.3	95.3

i^0_{corr} and i_{corr} represent the corrosion current density before and after the addition of corrosion inhibitor, respectively. The maximum corrosion inhibition efficiency η_p% after SVSE addition at all four temperature conditions is above 92%, and the results are closer to those calculated by EIS. This fully indicates that SVSE can be used as a good corrosion inhibitor for CS in HCl solution.

3.5. The Adsorption Isotherm Model

Six classical adsorption isotherm models were used to further investigate the adsorption behavior of SVSE on CS surfaces. The expressions for each model are as follows [56,57]:

$$\text{Langmuir}: \quad \frac{C_{inh}}{\theta} = \frac{1}{K_{ads}} + C_{inh} \tag{11}$$

$$\text{Temkin}: \quad exp^{(-2\alpha\theta)} = KC \tag{12}$$

$$\text{El–Awady}: \quad ln\frac{\theta}{1-\theta} = ylnC + lnK' \tag{13}$$

$$\text{Flory–Huggins}: \quad ln\frac{\theta}{C} = xln(1-\theta) + ln(xK_{ads}) \tag{14}$$

$$\text{Frumkin}: \quad ln\left[\frac{\theta}{(1-\theta)C}\right] = lnK + 2\alpha\theta \tag{15}$$

$$\text{Freundlich}: \quad log\theta = nlogC_{inh} + logK_{ads} \tag{16}$$

where K_{ads} denotes the adsorption equilibrium constant. C_{inh} represents the corrosion inhibitor concentration, α is the lateral interaction parameter between the adsorbed molecules, x is the number of adsorbed water molecules replaced by the molecules of the number of adsorbed water molecules replaced by inhibitor molecules, y is the number of inhibitor molecules adsorbed at a given active site and θ is the surface coverage. The results of the correlation fit are shown in Figure 7. In general, the model is considered to be satisfied when the R^2 of the fitted model is greater than 0.96 [50]. Therefore, the adsorption of SVSE on the CS surface is consistent with the Langmuir model.

The adsorption type of SVSE can be determined by calculating the value of standard free energy ΔG^0_{ads} with the following formula [58]:

$$\Delta G^0_{ads} = -RTln\left(10^6 K_{ads}\right) \tag{17}$$

where R represents the gas constant (8.314 J·mol^{-1}·K^{-1}), T is the absolute temperature (298.15 K), and 10^3 represents the concentration of water molecules (10^3 mg/L). The K_{ads} values of SVSE at 298–313 K were calculated to be 0.297, 0.367, 0.434 and 0.304, respectively, and the G^0_{ads} values were −31.264, −31.761, −32.175 and −31.291, respectively. In general, values of G^0_{ads} between −40 kJ/mol and −20 kJ/mol are considered as mixed adsorption [59]. Therefore, the adsorption of SVSE on the CS surface is a combination of chemisorption and physical adsorption.

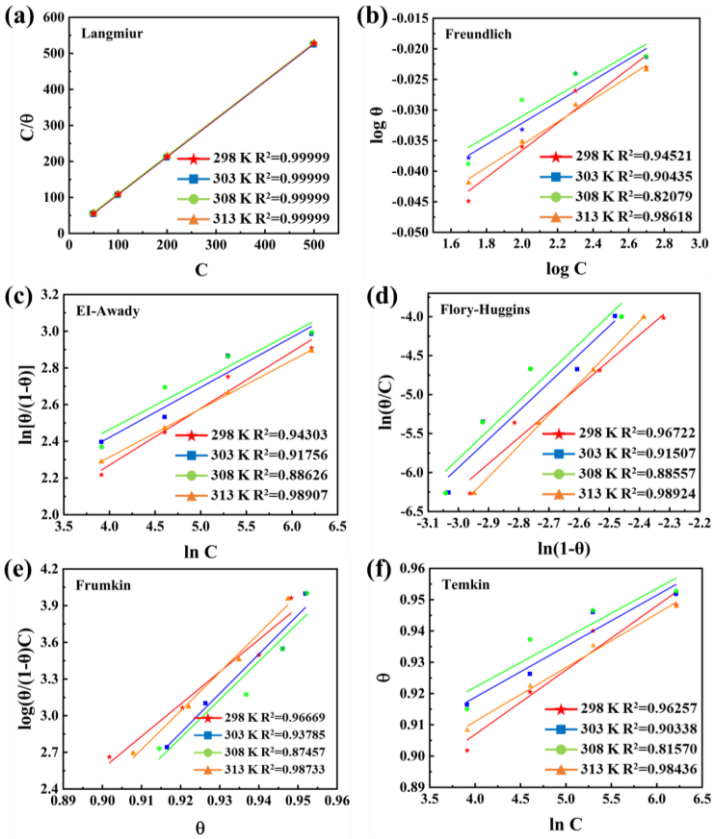

Figure 7. Six different adsorption isotherms. (**a**) Langmiur, (**b**) Freundlich, (**c**) EI-Awady, (**d**) Flory-Huggins, (**e**) Frumkin, (**f**) Temkin.

3.6. Surface Characterization

SEM images of samples immersed in 1 M HCl containing and not containing 500 mg/L SVSE for 2 h under different temperature conditions are shown in Figure 8. It can be seen that the surface of the CS immersed in 1 M HCl is riddled with white corrosion products and the corrosion is very severe. In contrast, under the same conditions, the addition of 500 mg/L SVSE of SVSE to the corrosion solution under the same conditions provides significant relief of the corrosion of CS and traces of sandpaper polishing can be observed on the surface. In addition, although the temperature increase accelerates the corrosion of CS, SVSE still exhibits corresponding corrosion inhibition performance. This indicates that SVSE can provide protection for CS at higher temperatures. The results of the SEM analysis well verified the findings of the electrochemical experiments.

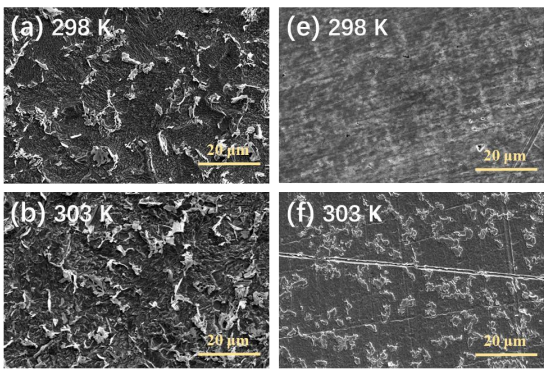

Figure 8. *Cont.*

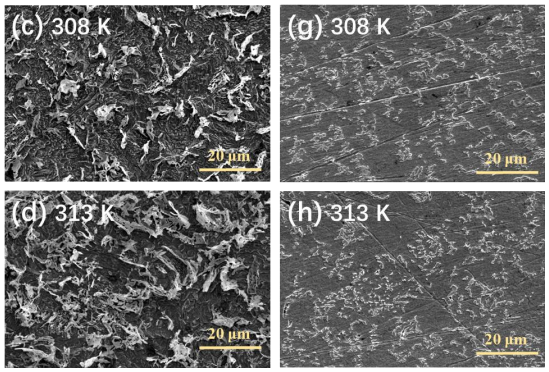

Figure 8. SEM images of CS immersed in 1 M HCl without corrosion inhibitor (**a**–**d**) and with 500 mg/L SVSE (**e**–**h**) for 2 h at different temperature conditions.

3.7. QC Analysis

Figure 9 shows the structures of the 14 amino acids with relatively high content in SVSE and their corresponding frontier molecular orbitals (HOMO and LUMO). HOMO and LUMO are related to the electron donating and electron accepting ability of the molecule, respectively [60]. From Figure 9, it can be seen that the HOMO of hydroxyl-containing amino acids serine, threonine, and tyrosine is mainly distributed on the amino and hydroxyl groups of the amino acids. The benzene ring on tyrosine and phenylalanine is also among the main distribution regions of HOMO. In contrast, the HOMO of other amino acids is mainly distributed on the amino and oxygen atoms. The LUMO orbitals are more evenly distributed, covering almost all oxygen atoms, nitrogen atoms and carbon atoms on the benzene ring. The distribution of HOMO and LUMO demonstrates the presence of active binding sites in these amino acid molecules and also indicates the potential corrosion inhibition ability of SVSE. Figure 10 shows the contour and surface plots of the electrostatic potential map (OESP) of the 14 amino acids, where the red and blue regions represent the more nucleophilic and electrophilic sites of the molecules, respectively. All the red regions are distributed near the oxygen and nitrogen atoms, indicating that this written position is the active reaction site [61].

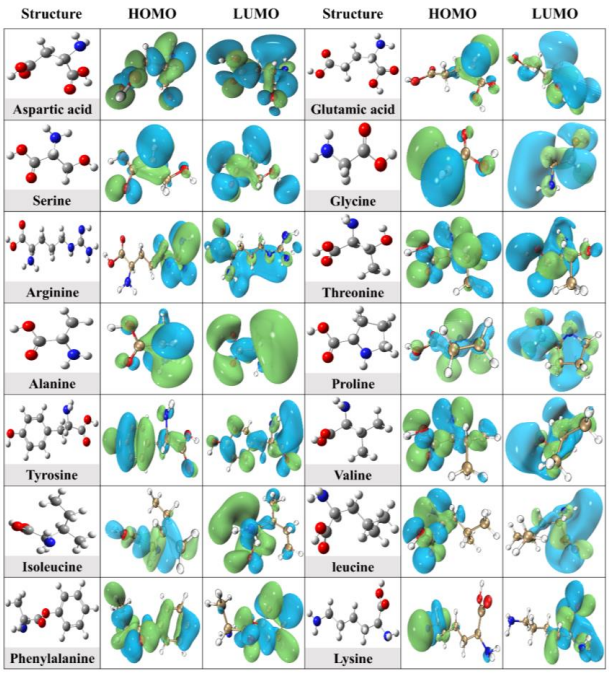

Figure 9. Optimized structures of 14 amino acid molecules, electronic distribution of HOMO and LUMO.

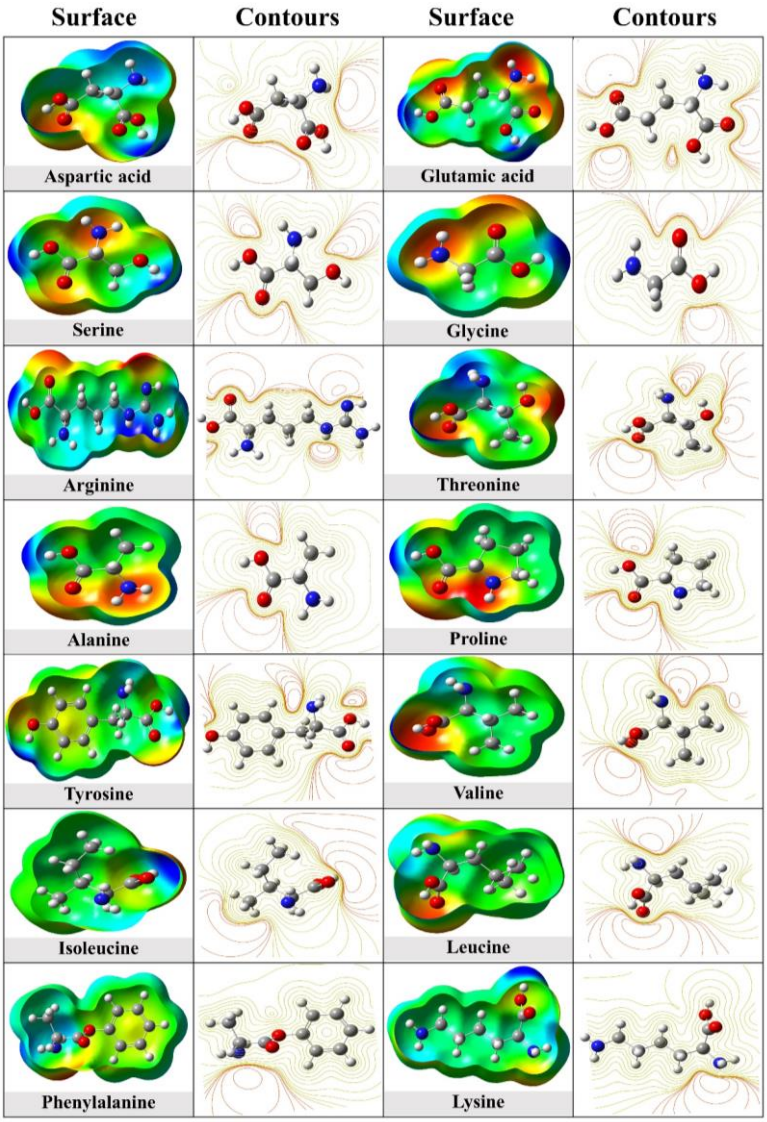

Figure 10. OESP diagram (surface and profile) of 14 amino acid molecules.

Table 5 shows the relevant calculation results. E_{HOMO} represents the energy of the most easily mobile electron in the molecule, and a smaller value indicates greater instability of the molecule. E_{LUMO} represents the energy of the most easily accepting electron in the molecule, and a smaller value indicates greater susceptibility to chemical reactions. ΔE refers to the energy difference between HOMO and LUMO, and a smaller ΔE value means the molecule is more easily excited to higher energy states and undergoes chemical reactions [62]. Similarly, for inhibitor molecules, a smaller ΔE value means the inhibitor molecule is more capable of providing electrons to form chemical bonds with the metal. The ΔE values of arginine, proline, and tyrosine are 5.61, 5.93, and 5.51, respectively, which are significantly smaller than those of other amino acid molecules. This implies that arginine, proline, and tyrosine may play a significant role in inhibiting metal corrosion. Dipole moment μ and electron transfer fraction ΔN are also considered by many researchers as key evaluation metrics. The values of μ and ΔN represent the magnitude of molecular polarity and the ability of charge transfer, and it is generally believed that larger values indicate easier adsorption of the inhibitor molecules on the metal surface [63]. Table 5 shows that the values of μ and ΔN for arginine are 5.26 and 0.61, respectively, which are significantly larger than those of other amino acids. This indicates that arginine is the most effective corrosion inhibitor among the active components of SVSE.

Table 5. Quantum chemical parameters of 14 amino acids.

Inhibitors	E_{HOMO} (eV)	E_{LUMO} (eV)	ΔE (eV)	I (eV)	A (eV)	χ (eV)	γ (eV)	μ (Debye)	ΔN
Aspartic acid	−7.23	−0.75	6.48	7.23	0.75	3.99	3.24	2.70	0.47
Glutamic acid	−7.01	−0.83	6.18	7.01	0.83	3.92	3.09	2.96	0.50
Serine	−6.95	−0.67	6.29	6.95	0.67	3.81	3.14	0.82	0.51
Glycine	−6.95	−0.59	6.37	6.95	0.59	3.77	3.18	2.12	0.51
Arginine	−6.37	−0.76	5.61	6.37	0.76	3.56	2.81	5.26	0.61
Threonine	−7.26	−0.79	6.47	7.26	0.79	4.03	3.24	2.96	0.46
Alanine	−6.89	−0.69	6.20	6.89	0.69	3.79	3.10	2.14	0.52
Proline	−6.49	−0.55	5.93	6.49	0.55	3.52	2.97	2.25	0.59
Tyrosine	−6.19	−0.69	5.51	6.19	0.69	3.44	2.75	0.95	0.65
Valine	−6.91	−0.53	6.38	6.91	0.53	3.72	3.19	1.60	0.51
Isoleucine	−7.07	−0.47	6.60	7.07	0.47	3.77	3.30	1.22	0.49
Leucine	−6.93	−0.53	6.40	6.93	0.53	3.73	3.20	1.54	0.51
Phenylalanine	−6.94	−0.67	6.27	6.94	0.67	3.81	3.13	2.44	0.51
Lysine	−6.66	−0.47	6.19	6.66	0.47	3.57	3.10	2.53	0.55

3.8. MDS Analysis

The side and top views of the adsorption results of individual inhibitor molecules on Fe (110) obtained through molecular dynamics simulations are shown in Figure 11. As the simulation progresses, the inhibitor molecules eventually adsorb on the metal surface in a parallel manner. Parallel adsorption helps reduce the exposed area of the CS, thereby reducing the corrosion caused by aggressive ions. Furthermore, the high binding energy ($E_{binding}$) between the corrosion inhibitor molecules and the metal surface is usually associated with excellent corrosion inhibition efficiency [64]. The calculated $E_{binding}$ values using Equations (7) and (8) are listed in Table 6. The $E_{binding}$ values of all SVSE molecules exceed 300, indicating the general corrosion inhibiting capability of these molecules. Arginine and tyrosine exhibit $E_{binding}$ values of 623 kJ/mol and 711 kJ/mol, respectively, which are significantly higher than those of other molecules. This suggests that arginine and tyrosine demonstrate relatively high corrosion inhibition performance.

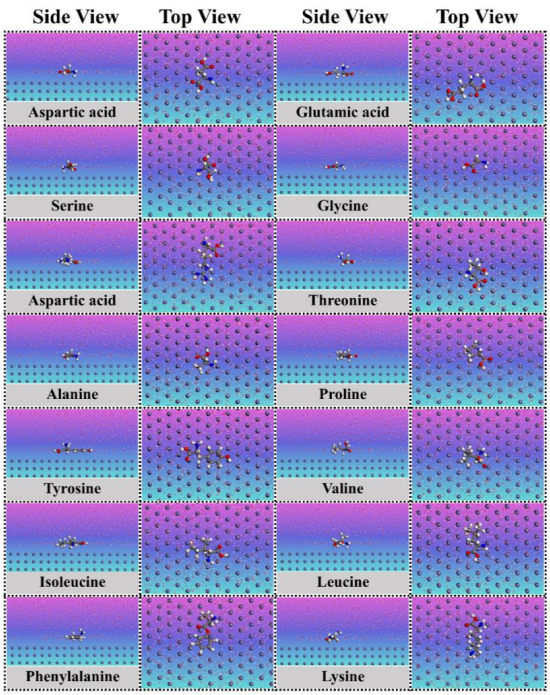

Figure 11. Equilibrium conformation of 14 amino acid molecules on the Fe (110) surface.

Table 6. Molecular dynamics simulation parameters of 14 amino acid molecules.

Compounds	E_{top} (kJ/mol)	E_{sub} (kJ/mol)	E_{inh} (kJ/mol)	$E_{interact}$ (kJ/mol)	$E_{binding}$ (kJ/mol)
Aspartic acid	−5139	−4611	−34	−494	494
Glutamic acid	−6686	−6213	11	−484	484
Serine	−4983	−4819	188	−352	352
Glycine	−4849	−4689	141	−294	301
Arginine	−5536	−4577	−336	−623	623
Threonine	−4900	−4659	169	−410	410
Alanine	−4822	−4665	156	−313	313
Proline	−4990	−4743	116	−362	362
Tyrosine	−5049	−4556	218	−711	711
Valine	−4833	−4658	194	−370	370
Isoleucine	−4910	−4714	238	−434	434
Leucine	−4947	−4648	106	−406	406
Phenylalanine	−4810	−4602	286	−493	493
Lysine	−5045	−4607	104	−541	541

3.9. Corrosion and Corrosion Inhibition Mechanism

When CS is immersed in HCl, an electrochemical reaction occurs, in which the iron at the anode is oxidized to Fe^{2+} and the hydrogen precipitation reaction occurs at the cathode to produce H_2 [65]:

Cathode:

$$Fe + H^+ \rightarrow \left(FeH^+\right)_{ads} \tag{18}$$

$$\left(FeH^+\right)_{ads} + e^- \rightarrow (FeH)_{ads} \tag{19}$$

$$(FeH)_{ads} + H^+ + e^- \rightarrow Fe + H_2 \tag{20}$$

Anode:

$$Fe + Cl^- \rightarrow \left(FeCl^-\right)_{ads} \tag{21}$$

$$\left(FeCl^-\right)_{ads} \rightarrow (FeCl)_{ads} + e^- \tag{22}$$

$$(FeCl)_{ads} \rightarrow \left(FeCl^+\right)_{ads} + e^- \tag{23}$$

$$FeCl^+ \rightarrow Fe^{2+} + Cl^- \tag{24}$$

The adsorption process of SVSE on the surface of CS includes physical and chemical adsorption, as shown in Figure 12. The iron atoms are oxidized to Fe^{2+}, and Cl^- are electrostatically adsorbed to the steel surface, resulting in a negatively charged surface. The main components of SVSE contain abundant amino groups, which are strong alkaline groups. They are easily protonated in HCl solution, forming positively charged substances that are readily adsorbed onto the negatively charged metal surface. In addition, the main components of SVSE are also rich in heteroatoms and unsaturated functional groups. These structures can form coordination bonds with the empty d orbitals of iron, leading to chemisorption [66]. SVSE undergoes both physical and chemical adsorption on the steel surface, effectively inhibiting the charge transfer process that causes corrosion on the steel surface. Therefore, it exhibits excellent inhibitory performance.

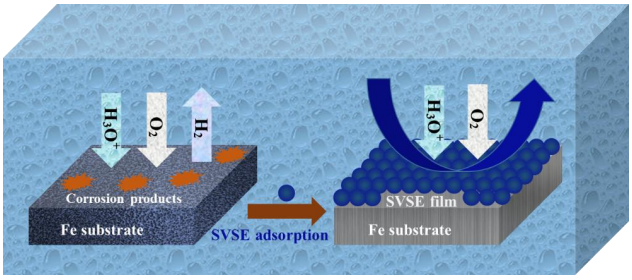

Figure 12. Mechanism of corrosion and corrosion inhibition of low CS in HCl.

4. Conclusions

The corrosion inhibition behavior of SVSE on CS in 1 M HCl was investigated by experiments and theoretical calculations. The main findings of this work are as follows:

(1) HPLC results showed that SVSE contains 18 amino acids, which are the main active molecules in SVSE. FTIR confirmed that SVSE contains O–H, C–H and N–H, which are consistent with the general characteristics of corrosion inhibitors.
(2) The electrochemical test results show that SVSE has good corrosion inhibition effect on CS in 1 M HCl, and the inhibition performance increases with increasing concentration and decreases with increasing temperature, which is a kind of mixed corrosion inhibitor with cathodic corrosion inhibition effect.
(3) The results of theoretical calculations show that the main components of SVSE have active adsorption sites and eventually adsorb on the CS substrate in a parallel manner, forming a protective film with high stability. The results of theoretical calculations effectively support the conclusions of experimental data.

Author Contributions: Conceptualization, Q.W. and Z.Y.; methodology, Q.W.; software, C.Z.; validation, Q.Z., H.Z. and X.Z.; formal analysis, C.Z., R.W. and Y.S.; investigation, Q.W. and C.Z.; resources, X.L.; data curation, C.Z. and Q.Z.; writing—original draft preparation, Q.W.; writing—review and editing, Z.Y.; visualization, C.Z.; supervision, Q.W.; project administration, Z.Y.; funding acquisition, Z.Y. All authors have read and agreed to the published version of the manuscript.

Funding: This work was supported by the Science and Technology Innovation Program of "the construction of the Chengdu–Chongqing economic circle" (No. KJCX2020050), the Research Foundation of Chongqing University of Science and Technology (No. ckrc2020025), the Natural Science Foundation of China (Nos. 51778097, 52178458), the Innovation Program for Graduate Students of Chongqing University of Science and Technology (No. YKJCX2220604, No. YKJCX2220605), and the Science and Technology Research Program of Chongqing Municipal Education Commission (Grant No. KJQN202201518).

Institutional Review Board Statement: Not applicable.

Informed Consent Statement: Not applicable.

Data Availability Statement: Not applicable.

Conflicts of Interest: The authors declare no conflict of interest.

Abbreviations

Abbreviation	Description
SVSE	Shell of *viviparid* snail extract
CS	Carbon steel
HPLC	High-performance liquid chromatography
FTIR	Fourier-transform infrared spectroscopy
QC	Quantum chemistry
MDS	Molecular dynamics simulations
EIS	Electrochemical impedance spectroscopy
PDP	Potentiodynamic polarization

References

1. Begum, A.; Vahith, R.; Kotra, V.; Shaik, M.R.; Khan, M. Spilanthes acmella Leaves Extract for Corrosion Inhibition in Acid Medium. *Coatings* **2021**, *11*, 106. [CrossRef]
2. Tian, Y.; Zhang, G.; Ye, H.; Zeng, Q.; Zhang, Z.; Tian, Z.; Jin, X.; Jin, N.; Chen, Z.; Wang, J. Corrosion of steel rebar in concrete induced by chloride ions under natural environments. *Constr. Build. Mater.* **2023**, *369*, 130504. [CrossRef]
3. Cai, F.; Huang, Y.; Xing, S.; Xu, Y.; Zhao, X.; Wang, X.; Wang, Z.; Ringsberg, J.W. Characteristics and mechanisms of low-alloy high-strength steel corrosion behavior under barnacle adhesion based on a comparison experiment. *Corros. Sci.* **2023**, *217*, 111146. [CrossRef]
4. Kairy, S.K.; Zhou, S.; Turnbull, A.; Hinds, G. Corrosion of pipeline steel in dense phase CO_2 containing impurities: A critical review of test methodologies. *Corros. Sci.* **2023**, *214*, 110986. [CrossRef]
5. Emelyanenko, K.A.; Emelyanenko, A.M.; Boinovich, L.B. Laser Obtained Superhydrophobic State for Stainless Steel Corrosion Protection, a Review. *Coatings* **2023**, *13*, 194. [CrossRef]
6. Zhang, W.; Li, C.; Wang, W.; Li, B.; Liu, X.; Liu, Y.; Guo, H.; Chen, S.; Feng, Y. Laminarin and sodium molybdate as efficient sustainable inhibitor for Q235 steel in sodium chloride solution. *Colloids Surf. A* **2022**, *637*, 128199. [CrossRef]
7. Wang, Q.; Zhang, Q.; Liu, L.; Zheng, H.; Wu, X.; Li, Z.; Gao, P.; Sun, Y.; Yan, Z.; Li, X. Experimental, DFT and MD evaluation of Nandina domestica Thunb. extract as green inhibitor for CS corrosion in acidic medium. *J. Mol. Struct.* **2022**, *1265*, 133367. [CrossRef]
8. Li, X.; Deng, S. Synergistic inhibition effect of walnut green husk extract and potassium iodide on the corrosion of cold rolled steel in trichloroacetic acid solution. *J. Mater. Res. Technol.* **2020**, *9*, 15604–15620. [CrossRef]
9. Zhang, W.; Nie, B.; Wang, M.; Shi, S.; Gong, L.; Gong, W.; Pang, H.; Liu, X.; Li, B.; Feng, Y.; et al. Chemically modified resveratrol as green corrosion inhibitor for Q235 steel: Electrochemical, SEM, UV and DFT studies. *J. Mol. Liq.* **2021**, *343*, 117672. [CrossRef]
10. Benzbiria, N.; Thoume, A.; Echihi, S.; Belghiti, M.E.; Elmakssoudi, A.; Zarrouk, A.; Azzi, M.; Zertoubi, M. Coupling of experimental and theoretical studies to apprehend the action of benzodiazepine derivative as a corrosion inhibitor of carbon steel in 1M HCl. *J. Mol. Struct.* **2023**, *1281*, 135139. [CrossRef]
11. Wang, Q.; Wang, R.; Zhang, Q.; Zhao, C.; Zhou, X.; Zheng, H.; Zhang, R.; Sun, Y.; Yan, Z. Application of Biomass Corrosion Inhibitors in Metal Corrosion Control: A Review. *Molecules* **2023**, *28*, 062832. [CrossRef]
12. Berrissoul, A.; Ouarhach, A.; Benhiba, F.; Romane, A.; Guenbour, A.; Dikici, B.; Bentiss, F.; Zarrouk, A.; Dafali, A. Assessment of corrosion inhibition performance of origanum compactum extract for mild steel in 1 M HCl: Weight loss, electrochemical, SEM/EDX, XPS, DFT and molecular dynamic simulation. *Ind. Crops Prod.* **2022**, *187*, 115310. [CrossRef]
13. Farag, A.A.; Ismail, A.S.; Migahed, M.A. Environmental-friendly shrimp waste protein corrosion inhibitor for carbon steel in 1 M HCl solution. *Egypt. J. Pet.* **2018**, *27*, 1187–1194. [CrossRef]
14. Wang, Q.; Liu, L.; Zhang, Q.; Wu, X.; Zheng, H.; Gao, P.; Zeng, G.; Yan, Z.; Sun, Y.; Li, Z.; et al. Insight into the anti-corrosion performance of Artemisia argyi leaves extract as eco-friendly corrosion inhibitor for carbon steel in HCl medium. *Sustain. Chem. Pharm.* **2022**, *27*, 100710. [CrossRef]
15. Lin, B.; Shao, J.; Zhao, C.; Zhou, X.; He, F.; Xu, Y. Passiflora edulis Sims peel extract as a renewable corrosion inhibitor for mild steel in phosphoric acid solution. *J. Mol. Liq.* **2023**, *375*, 121296. [CrossRef]
16. Song, Z.; Donkor, S.; Zhang, Y.; Liu, Q.; Liu, Y.; Na, X.; Cai, H.; Odoom, J.K. Adsorption and corrosion inhibition performance of rice bran extract on carbon steel in aqueous chloride solution: Experimental, computational and theoretical studies. *Constr. Build. Mater.* **2023**, *363*, 129801. [CrossRef]
17. Akrom, M.; Saputro, A.G.; Maulana, A.L.; Ramelan, A.; Nuruddin, A.; Rustad, S.; Dipojono, H.K. DFT and microkinetic investigation of oxygen reduction reaction on corrosion inhibition mechanism of iron surface by Syzygium Aromaticum extract. *Appl. Surf. Sci.* **2023**, *615*, 156319. [CrossRef]
18. Praveen, B.M.; Alhadhrami, A.; Hebbar, N.; Prabhu, R. Anti-Corrosion Behavior of Olmesartan for Soft-Cast Steel in 1 mol dm^{-3} HCl. *Coatings* **2021**, *11*, 965. [CrossRef]
19. Ganjoo, R.; Sharma, S.; Thakur, A.; Assad, H.; Kumar, S.P.; Dagdag, O.; Berisha, A.; Seydou, M.; Ebenso, E.E.; Kumar, A. Experimental and theoretical study of Sodium Cocoyl Glycinate as corrosion inhibitor for mild steel in hydrochloric acid medium. *J. Mol. Liq.* **2022**, *364*, 119988. [CrossRef]
20. Rajamohan, N.; Al Shibli, F.S.Z.S.; Rajasimman, M. Environmentally benign Prosopis juliflora extract for corrosion protection by sorption—Gravimetric, mechanistic and thermodynamic studies. *Environ. Res.* **2022**, *203*, 111816. [CrossRef]
21. Setiawan, K.A.P.; Wahyuadi, S.J.; Wahyu, M.; Syaiful, A.M.; Ahmad, M.; Aga, R.; Rini, R. Insight on Corrosion Prevention of C1018 in 1.0 M Hydrochloric Acid Using Liquid Smoke of Rice Husk Ash: Electrochemical, Surface Analysis, and Deep Learning Studies. *Coatings* **2023**, *13*, 136. [CrossRef]
22. Thomas, A.; At, J.R.; Joseph, A. Extended protection of mild steel in molar HCl using the Garcinia Indica fruit rind extract (GIW) and iodide ions; electrochemical, thermodynamic and kinetic studies. *J. Indian Chem. Soc.* **2021**, *98*, 100167. [CrossRef]
23. Tang, M.; Li, X.; Deng, S.; Lei, R. Synergistic inhibition effect of Mikania micrantha extract with KI on steel corrosion in H_2SO_4 solution. *J. Mol. Liq.* **2021**, *344*, 117926. [CrossRef]
24. Majd, M.T.; Ramezanzadeh, M.; Bahlakeh, G.; Ramezanzadeh, B. Steel corrosion lowering in front of the saline solution by a nitrogen-rich source of green inhibitors: Detailed surface, electrochemical and computational studies. *Constr. Build. Mater.* **2020**, *254*, 119266. [CrossRef]

25. Mansha, M.; Madhan, K.A.; Adesina, A.Y.; Obot, I.B.; Khan, M. A novel trans-esterified water soluble hyperbranched polymer for surface protection of X60 steel: Experimental and theoretical approach. *J. Mol. Liq.* **2022**, *349*, 118091. [CrossRef]
26. Nkiko, M.O. Evaluating the Deterioration of Galvanized Steel in an Acidic Medium using Pinus Oocarpa Seed Extract as Inhibitor. *Port. Electrochim. Acta* **2022**, *40*, 79–87. [CrossRef]
27. Wang, Q.; Wu, X.; Zheng, H.; Xiao, X.; Liu, L.; Zhang, Q.; Gao, P.; Yan, Z.; Sun, Y.; Li, Z.; et al. Insight into anti-corrosion behavior of Centipeda minima leaves extract as high-efficiency and eco-friendly inhibitor. *Colloids Surf. A* **2022**, *640*, 128458. [CrossRef]
28. Zhu, M.; Guo, L.; Chang, J.; He, Z.; Yao, Y.; Zhang, R.; Zheng, X.; Marzouki, R. Synergistic effect of 4-dimethylaminopyridine with sodium dodecyl sulfonate and potassium bromide on the corrosion inhibition of mild steel in HCl medium: A collective experimental and computational investigation. *J. Adhes. Sci. Technol.* **2021**, *36*, 2462–2477. [CrossRef]
29. Kuznetsov, Y.I.; Redkina, G. Thin Protective Coatings on Metals Formed by Organic Corrosion Inhibitors in Neutral Media. *Coatings* **2022**, *12*, 149. [CrossRef]
30. Al-Amiery, A.A.; Isahak, W.N.R.W.; Al-Azzawi, W.K. Corrosion Inhibitors: Natural and Synthetic Organic Inhibitors. *Lubricants* **2023**, *11*, 040174. [CrossRef]
31. Jie, Y.; Zhongheng, L.; Jinfa, S.; Zhenwei, Y. Study on the corrosion inhibition performance of sodium silicate and polyaspartic acid for 35CrMo steel. *Int. J. Electrochem. Sci.* **2023**, *18*, 100042. [CrossRef]
32. Verma, C.; Hussain, C.M.; Quraishi, M.A.; Alfantazi, A. Green surfactants for corrosion control: Design, performance and applications. *Adv. Colloid Interface Sci.* **2023**, *311*, 102822. [CrossRef] [PubMed]
33. Thakur, A.; Kaya, S.; Abousalem, A.S.; Sharma, S.; Ganjoo, R.; Assad, H.; Kumar, A. Computational and experimental studies on the corrosion inhibition performance of an aerial extract of Cnicus Benedictus weed on the acidic corrosion of mild steel. *Process Saf. Environ. Prot.* **2022**, *161*, 801–818. [CrossRef]
34. Dehghani, A.; Bahlakeh, G.; Ramezanzadeh, B. Green Eucalyptus leaf extract: A potent source of bio-active corrosion inhibitors for mild steel. *Bioelectrochemistry* **2019**, *130*, 107339. [CrossRef]
35. Li, X.; Deng, S.; Fu, H. Inhibition of the corrosion of steel in HCl, H_2SO_4 solutions by bamboo leaf extract. *Corros. Sci.* **2012**, *62*, 163–175. [CrossRef]
36. Chen, S.; Zhao, H.; Chen, S.; Wen, P.; Wang, H.; Li, W. Camphor leaves extract as a neoteric and environment friendly inhibitor for Q235 steel in HCl medium: Combining experimental and theoretical researches. *J. Mol. Liq.* **2020**, *312*, 113433. [CrossRef]
37. Suriya, P.A.; Kavitha, K.; Benita, S.H.; Susai, R. Inhibition of corrosion of mild steel in simulated oil well water by an aqueous extract of Andrographis paniculata. *Indian J. Chem. Technol.* **2020**, *27*, 113433.
38. Abhradip, P.; Chandan, D. New eco-friendly anti-corrosion inhibitor of purple rice bran extract for boiler quality steel: Experimental and theoretical investigations. *J. Mol. Struct.* **2022**, *1251*, 131988. [CrossRef]
39. Zouarhi, M.; Chellouli, M.; Abbout, S.; Hammouch, H.; Dermaj, A.; Hassane, S.O.S.; Decaro, P.; Bettach, N.; Hajjaji, N.; Srhiri, A. Inhibiting Effect of a Green Corrosion Inhibitor Containing Jatropha Curcas Seeds Oil for Iron in an Acidic Medium. *Port. Electrochim. Acta.* **2018**, *36*, 179–195. [CrossRef]
40. Pradipta, I.; Kong, D.; Tan, J.B.L. Natural organic antioxidants from green tea inhibit corrosion of steel reinforcing bars embedded in mortar. *Constr. Build. Mater.* **2019**, *227*, 351–362. [CrossRef]
41. Eddy, O.N. Adsorption and inhibitive properties of ethanol extract of Garcinia kola and Cola nitida for the corrosion of mild steel in H_2SO_4. *Pigm. Resin Technol.* **2010**, *39*, 348–354. [CrossRef]
42. Elqars, E.; Guennoun, M.; Aicha, O.; Sqalli Houssini, N.; Elhafdi, M.; Essadki, A.; Ait chaoui, M.; Nbigui, T.; Singh, A.K. Expired Chicken Egg-White Extract's Adsorption Behavior As a Corrosion Inhibitor for CS in 1 M HCl. *Acad. J. Chem.* **2021**, *2021*, 3416092. [CrossRef]
43. Zhang, Q.H.; Hou, B.S.; Zhang, G.A. Inhibitive and adsorption behavior of thiadiazole derivatives on carbon steel corrosion in CO_2-saturated oilfield produced water: Effect of substituent group on efficiency. *J Colloid Interface Sci.* **2020**, *572*, 91–106. [CrossRef] [PubMed]
44. Zhang, Q.H.; Hou, B.S.; Li, Y.Y.; Lei, Y.; Wang, X.; Liu, H.F.; Zhang, G.A. Two amino acid derivatives as high efficient green inhibitors for the corrosion of carbon steel in CO_2-saturated formation water. *Corros. Sci.* **2021**, *189*, 109596. [CrossRef]
45. Zaher, A.; Aslam, R.; Lee, H.S.; Khafouri, A.; Boufellous, M.; Alrashdi, A.A.; El aoufir, Y.; Lgaz, H.; Ouhssine, M. A combined computational & electrochemical exploration of the *Ammi visnaga* L. extract as a green corrosion inhibitor for carbon steel in HCl solution. *Arab. Acad. J. Chem.* **2022**, *15*, 103573. [CrossRef]
46. Zhang, D.; Tang, Y.; Qi, S.; Dong, D.; Cang, H.; Lu, G. The inhibition performance of long-chain alkyl-substituted benzimidazole derivatives for corrosion of mild steel in HCl. *Corros. Sci.* **2016**, *102*, 517–522. [CrossRef]
47. Shafek, S.H.; Ghiaty, E.A.; El Basiony, N.M.; Badr, E.A.; Shaban, S.M. Preparation of zwitterionic ionic surfactants-based sulphonyl for steel protections: Experimental and theoretical insights. *Z. Phys. Chem.* **2023**, *237*, 1–33. [CrossRef]
48. Olawale, O.; Bello, J.O.; Ogunsemi, B.T.; Uchella, U.C.; Oluyori, A.P.; Oladejo, N.K. Optimization of chicken nail extracts as corrosion inhibitor on mild steel in 2 M H_2SO_4. *Heliyon* **2019**, *5*, e02821. [CrossRef]
49. Saady, A.; Rais, Z.; Benhiba, F.; Salim, R.; Ismaily, A.K.; Arrousse, N.; Elhajjaji, F.; Taleb, M.; Jarmoni, K.; Kandri, R.Y.; et al. Chemical, electrochemical, quantum, and surface analysis evaluation on the inhibition performance of novel imidazo [4,5-b] pyridine derivatives against mild steel corrosion. *Corros. Sci.* **2021**, *189*, 109621. [CrossRef]
50. Yeganeh, M.; Rezvani, M.H.; Laribaghal, S.M. Electrochemical behavior of additively manufactured 316L stainless steel in H_2SO_4 solution containing methionine as an amino acid. *Colloids Surf. A* **2021**, *627*, 127120. [CrossRef]

51. Yang, X.; Fu, S.; Wang, Q.; Sun, Q.; Zhang, J.; Peng, Y.; Liang, Z.; Li, J. Protective behaviour of naphthylamine derivatives for steel reinforcement in the simulated concrete pore solutions: Detailed experimental and computational explorations. *J. Mol. Struct.* **2022**, *1270*, 133898. [CrossRef]
52. Salinas-Solano, G.; Porcayo-Calderon, J.; Martinez de la Escalera, L.M.; Canto, J.; Casales-Diaz, M.; Sotelo-Mazon, O.; Henao, J.; Martinez-Gomez, L. Development and evaluation of a green corrosion inhibitor based on rice bran oil obtained from agro-industrial waste. *Ind. Crops Prod.* **2018**, *119*, 111–124. [CrossRef]
53. Wang, Q.; Zheng, H.; Liu, L.; Zhang, Q.; Wu, X.; Yan, Z.; Sun, Y.; Li, X. Insight into the anti-corrosion behavior of Reineckia Carnea leaves extract as an eco-friendly and high-efficiency corrosion inhibitor. *Ind. Crops Prod.* **2022**, *188*, 115640. [CrossRef]
54. Wan, S.; Wei, H.; Quan, R.; Luo, Z.; Wang, H.; Liao, B.; Guo, X. Soybean extract firstly used as a green corrosion inhibitor with high efficacy and yield for carbon steel in acidic medium. *Ind. Crops Prod.* **2022**, *187*, 115354. [CrossRef]
55. Solomon, M.M.; Essien, K.E.; Loto, R.T.; Ademosun, O.T. Synergistic corrosion inhibition of low CS in HCl and H_2SO_4 media by 5-methyl-3-phenylisoxazole-4-carboxylic acid and iodide ions. *J. Adhes. Sci. Technol.* **2021**, *36*, 1200–1226. [CrossRef]
56. Corrales-Luna, M.; Le Manh, T.; Romero-Romo, M.; Palomar-Pardavé, M.; Arce-Estrada, E.M. 1-Ethyl 3-methylimidazolium thiocyanate ionic liquid as corrosion inhibitor of API 5L X52 steel in H_2SO_4 and HCl media. *Corros. Sci.* **2019**, *153*, 85–99. [CrossRef]
57. Cui, L.; Hang, M.; Huang, H.; Gao, X. Experimental study on multi-component corrosion inhibitor for steel bar in chloride environment. *Constr. Build. Mater.* **2021**, *313*, 125533. [CrossRef]
58. Helal, N.H.; Badawy, W.A. Environmentally safe corrosion inhibition of Mg-Al-Zn alloy in chloride free neutral solutions by amino acids. *Electrochim. Acta.* **2011**, *56*, 6581–6587. [CrossRef]
59. Hou, B.S.; Zhang, Q.H.; Li, Y.Y.; Zhu, G.Y.; Lei, Y.; Wang, X.; Liu, H.F.; Zhang, G.A. In-depth insight into the inhibition mechanism of pyrimidine derivatives on the corrosion of carbon steel in CO_2-containing environment based on experiments and theoretical calculations. *Corros. Sci.* **2021**, *181*, 109236. [CrossRef]
60. Prasad, D.; Singh, R.; Kaya, S.; el Ibrahimi, B. Natural corrosion inhibitor of renewable eco-waste for SS-410 in sulfuric acid medium: Adsorption, electrochemical, and computational studies. *J. Mol. Liq.* **2022**, *351*, 118671. [CrossRef]
61. Rbaa, M.; Fardioui, M.; Verma, C.; Abousalem, A.S.; Galai, M.; Ebenso, E.E.; Guedira, T.; Lakhrissi, B.; Warad, I.; Zarrouk, A. 8-Hydroxyquinoline based chitosan derived carbohydrate polymer as biodegradable and sustainable acid corrosion inhibitor for mild steel: Experimental and computational analyses. *Int. J. Biol. Macromol.* **2020**, *155*, 645–655. [CrossRef] [PubMed]
62. Yan, T.; Zhang, S.; Feng, L.; Qiang, Y.; Lu, L.; Fu, D.; Wen, Y.; Chen, J.; Li, W.; Tan, B. Investigation of imidazole derivatives as corrosion inhibitors of copper in sulfuric acid: Combination of experimental and theoretical researches. *J. Taiwan Inst. Chem. Eng.* **2020**, *106*, 118–129. [CrossRef]
63. Pal, A.; Das, C. A novel use of solid waste extract from tea factory as corrosion inhibitor in acidic media on boiler quality steel. *Ind. Crops Prod.* **2020**, *151*, 112468. [CrossRef]
64. Singh, A.; Ansari, K.R.; Ituen, E.; Guo, L.; Abdul, W.M.; Quraishi, M.A.; Kong, X.; Lin, Y. A new series of synthesized compounds as corrosion mitigator for storage tanks: Detailed electrochemical and theoretical investigations. *Constr. Build. Mater.* **2020**, *259*, 120421. [CrossRef]
65. Wan, S.; Zhang, T.; Chen, H.; Liao, B.; Guo, X. Kapok leaves extract and synergistic iodide as novel effective corrosion inhibitors for Q235 carbon steel in H_2SO_4 medium. *Ind. Crops Prod.* **2022**, *178*, 114649. [CrossRef]
66. Hou, B.S.; Xu, N.; Zhang, Q.H.; Xuan, C.J.; Liu, H.F.; Zhang, G.A. Effect of benzyl substitution at different sites on the inhibition performance of pyrimidine derivatives for mild steel in highly acidic solution. *J. Taiwan Inst. Chem. Eng.* **2019**, *95*, 541–554. [CrossRef]